Journal of the European Ceramic Society 22 (2002) 527–534

www.elsevier.com/locate/jeurceramsoc

The effect of additives on sintering behavior and strength retention in silicon nitride with RE-disilicate

Z.L. Hong[a,*], H. Yoshida[b], Y. Ikuhara[c], T. Sakuma[b], T. Nishimura[d], M. Mitomo[d]

[a]*Department of Materials Science, Graduate School of Engineering, The University of Tokyo, 7-3-1 Hongo, Bunkyo-ku, Tokyo, 113-8656 Japan*
[b]*Department of Advanced Materials Science, Graduate School of Frontier Science, The University of Tokyo, 7-3-1 Hongo, Bunkyo-ku, Tokyo, 113-8656 Japan*
[c]*Engineering Research Institute, School of Engineering, The University of Tokyo, 7-3-1 Hongo, Bunkyo-ku, Tokyo, 113-8656 Japan*
[d]*National Institute for Research in Inorganic Materials, 1-1 Namiki, Tsukuba-shi, Ibaraki, 305 Japan*

Accepted 21 April 2001

Abstract

Four kinds of Si_3N_4–$RE_2Si_2O_7$ (RE: Nd, Sm, Y, Yb) ceramics have been fabricated by hot pressing at 1725–1750°C for 2 h in N_2 gas flow and post-annealing at 1450°C for 4 h. The effect of rare-earth oxide additions on the densification process was investigated by measuring the shrinkage of the compact. Results revealed that the rare-earth oxides affect the densification process of Si_3N_4–$RE_2Si_2O_7$ ceramics in which the shrinkage temperature varies with the types of rare-earth additives. The Si–RE–O–N liquid phase formation temperature can be estimated from the onset temperature of final shrinkage stage, and the temperature is in the order of Sm < Nd < Y < Yb. Flexural strength was examined at temperature in a range of 25–1600°C in N_2 gas flow. The high temperature strength of Si_3N_4–$Yb_2Si_2O_7$ or Si_3N_4–$Y_2Si_2O_7$ ceramics is better than that of Si_3N_4–$Sm_2Si_2O_7$ or Si_3N_4–$Nd_2Si_2O_7$ ceramics. There is a roughly linear relation between the strength retention and the liquid phase formation temperature. Present results indicate that Si_3N_4–$RE_2Si_2O_7$ ceramics with high strength retention can be fabricated by adopting additives with small ionic radius and high ionic charge.

Keywords: Grain boundaries; Hot-pressing; Mechanical properties; Si_3N_4; Strength

1. Introduction

High temperature mechanical properties in silicon nitride ceramics is degraded by the presence of a grain boundary amorphous phase resulting from a liquid phase sintering process.[1,2] In order to prevent the degradation in the high temperature strength, much effort, such as selecting refractory oxides as additives,[3] crystallizing the amorphous grain pocket phase,[4,5] and adopting the transient liquid phase sintering,[6] has been made.

Silicon nitride ceramics for high-temperature use are usually fabricated by selecting the refractory rare-earth oxides (Re_2O_3) as additives and the $Re_2Si_2O_7$ phase is crystallized as a grain boundary phase by post-annealing.[7–9] The good high temperature mechanical properties are supposed to be related to the refractory nature of the grain boundary phase that is crystallized after sintering. In previous reports, the strength retention at 1300°C in Si_3N_4–$Re_2Si_2O_7$ materials was discussed in terms of the Re_2O_3–SiO_2 binary eutectic temperature.[9] On the other hand, Choi et al.[10] reported that the high temperature strength at 1200°C is correlated with the cationic radius of the oxide additives. Nevertheless, in Si_3N_4–$Re_2Si_2O_7$ materials, no results have been reported about the effect of the additives on the densification behavior and, the correlation between the densification behavior and the strength retention. This paper aims to examine the densification behavior and the flexural strength up to 1600°C in four kinds of Si_3N_4 ceramics with the grain boundary phase of $Re_2Si_2O_7$ (Re: Nd, Sm, Y, Yb). The effect of Re_2O_3 additives on the densification and strength retention behavior is discussed from the view point of liquid phase formation temperature.

2. Experimental procedure

Four kinds of rare-earth oxides, Nd_2O_3, Sm_2O_3, Yb_2O_3, and Y_2O_3 were selected as the sintering aid. The composition chosen for the study is Si_3N_4 –5 mol% Re_2O_3 –10 mol% SiO_2, which lies on the subsolidus Si_3N_4–$Re_2Si_2O_7$

* Corresponding author.
E-mail address: hong@ceramic.mm.t.u-tokyo.ac.jp (Z.L. Hong).

0955-2219/02/$ - see front matter
PII: S0955-2219(01)00298-9

phase tie line based on reported phase diagrams.[11] Si_3N_4 with about 10 vol. % $Re_2Si_2O_7$ will be fabricated if the additives could be completely crystallized.

The starting materials were Si_3N_4 powders (SN-E10, Ube Industries, Tokyo, Japan), Re_2O_3 powders (99.99%, Shin-Etsu Chemical Co. Ltd. Tokyo, Japan), and SiO_2 powders (high-purity grade, Wako Pure Chemical Ind. Ltd. Osaka, Japan). The raw powders were mixed by planetary ball mill for 2 h in hexane, using a pot and ball made of silicon nitride. After the ball milling, the powder mixtures were dried, ground, and sieved.

The powder mixture was hot pressed at 1725–1750°C for 2 h under a pressure of 20 MPa in N_2 atmosphere. The sintering condition is shown in Table 1. The die was coated with h-BN powder to prevent the reaction between powders and the die. The heating schedule was 30°C/min from room temperature to 1000°C followed by 10°C/min to 1725–1750°C. After 2 h holding, the specimen was allowed to cool to 1450°C and held at this temperature for 4 h under N_2 atmosphere to crystallize the $Re_2Si_2O_7$ phase. The shrinkage of powder compact was monitored by a displacement of the pressing ram. A shrinkage curve was obtained by subtracting the thermal expansion of the entire loading train from raw data. Quenched samples were prepared by heating the samples to target temperature and holding for 0 and 2 h, respectively. Then the furnace was shut off with a cooling rate of about 100°C/min.

Sample density was measured using the Archimedes method. The phase identification was conducted by X-ray diffraction analysis (Rigaku, Rint 2000, Japan). The surfaces of specimens were polished and plasma-etched by CF_4 containing 7.8% O_2 for a scanning electron microscopy (JSM-5200, Jeol, Tokyo, Japan) observation. The diameter and length of each grain were measured from the SEM micrographs including more than 500 grains. The aspect ratio of each grain was estimated as the ratio of length to diameter. The average value of the top 10% aspect ratio was estimated as the aspect ratio of each material. High-resolution electron microscopy (HREM; H9000NAR, Hitachi, Japan) observations were also performed to examine the grain boundary structure.

A four-point bending test was conducted at a temperature in a range from room temperature to 1600°C at the cross-head speed of 0.50 mm/s. The size of the specimen was $3\times2.5\times25$ mm^3. The tensile surface and edges were finally polished with 1 μm diamond polishing slurry. The inner span and out span of the testing jig was 10 and 20 mm, respectively. Five specimens from different pellets were used and the average value was calculated for each temperature.

3. Results and discussion

Fig. 1 shows the XRD profiles of present materials. In present four materials, XRD results revealed that β-Si_3N_4 is the major phase and $Re_2Si_2O_7$ phase is the secondary phase. The composition and properties in the present materials are shown in Table 1. As shown in Table 1, the relative density is about or more than 99% of the theoretical density which is assumed that almost all additives become $Re_2Si_2O_7$ phase. Fig. 2 is the typical SEM micrographs of four materials. SEM results indicate that four materials have nearly similar microstructure. Fig. 3 is

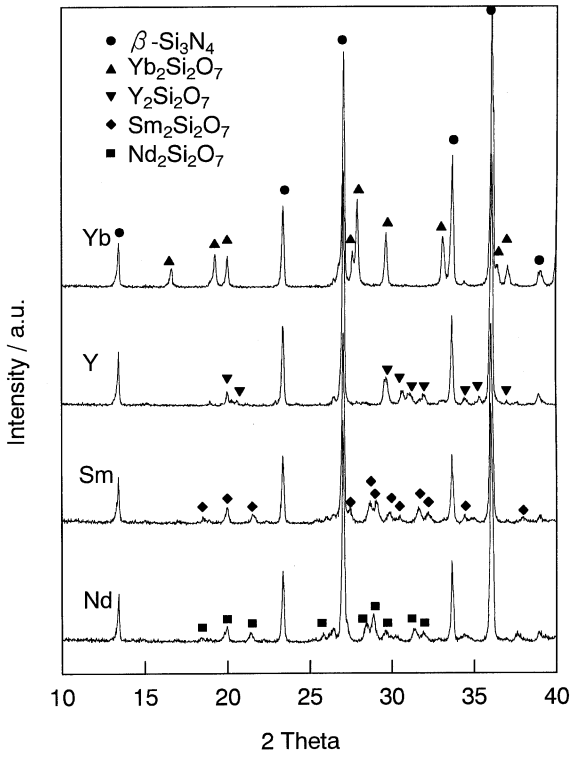

Fig. 1. XRD patterns of prepared samples showing the crystallization of $Re_2Si_2O_7$ as the secondary phase (Re: Nd, Sm, Y, Yb).

Table 1
Composition and properties of the Si_3N_4-10 vol. % $Re_2Si_2O_7$ (Re = Nd, Sm, Y, Yb) ceramics

Materials	Si_3N_4–SiO_2–Re_2O_3 (mol%)	Sintering temperature (°C)	Relative density (%)	Average grain diameter (μm)	Aspect ratio
Si_3N_4–$Nd_2Si_2O_7$	85.09–9.94–4.97	1725	98.7	0.40	4.5
Si_3N_4–$Sm_2Si_2O_7$	84.85–10.1–5.05	1725	98.9	0.44	4.8
Si_3N_4–$Y_2Si_2O_7$	85.48–9.68–4.84	1750	99.7	0.42	5.0
Si_3N_4–$Yb_2Si_2O_7$	85.06–9.96–4.98	1750	99.8	0.48	4.6

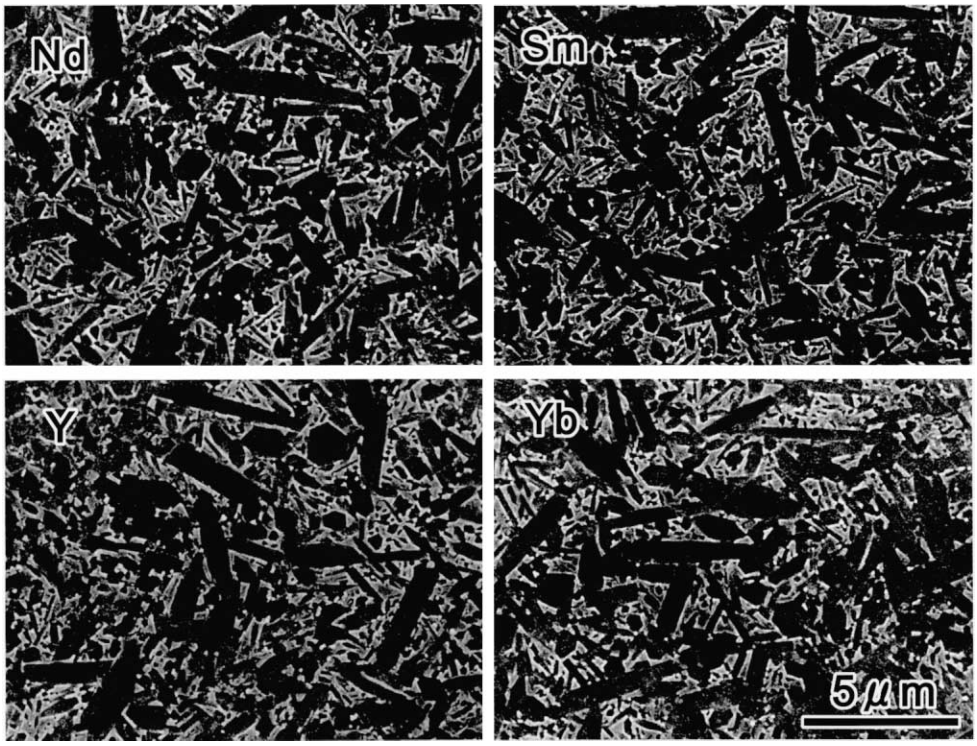

Fig. 2. SEM micrographs showing similar microstructure characteristics for Si_3N_4–$Re_2Si_2O_7$ ceramics (Re: Nd, Sm, Y, Yb).

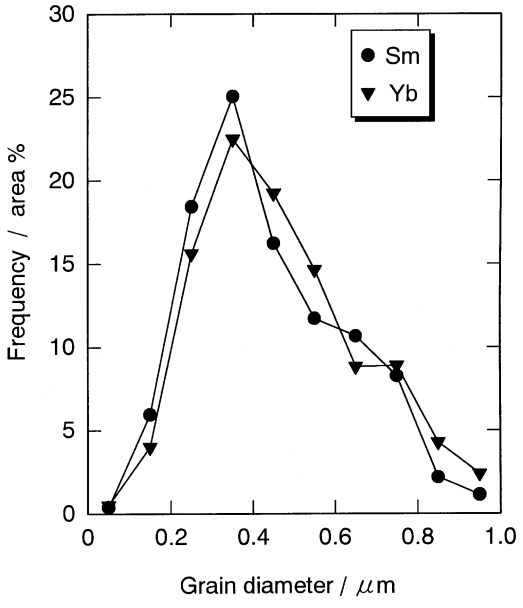

Fig. 3. Distribution of area frequency as a function of grain diameter showing no obvious difference in Si_3N_4–$Sm_2Si_2O_7$ and Si_3N_4–$Yb_2Si_2O_7$ ceramics.

the grain size distribution result in Si_3N_4–$Sm_2Si_2O_7$ and Si_3N_4–$Yb_2Si_2O_7$ ceramics. The frequency of surface area means the proportion of cross-sectional area of grains with a same diameter to total area of the surface observed by SEM. In Si_3N_4 ceramics, this type of plot is the most suitable plot for the characterization of grain size distribution in the materials consisting of large elongated grains because the standard plot of grain number can not reflect the presence of large elongated grains.[12] As shown in Fig. 3, no obvious difference was found about the grain size distribution between Si_3N_4–$Sm_2Si_2O_7$ and Si_3N_4–$Yb_2Si_2O_7$ ceramics that show the biggest difference in room temperature strength among present materials. The results of average grain diameter and aspect ratio in four materials are shown in Table 1. In the present materials, the average grain diameter varies from 0.40 to 0.48 μm and the aspect ratio varies from 4.5 to 5.0. The above results demonstrate that there is no obvious difference in microstructure among these four materials.

The effect of various rare-earth additives on the densification process has not been reported, although the densification process was studied extensively in such Si_3N_4 ceramics as SiAlON ceramics and Y_2O_3–fluxed Si_3N_4.[13,14] In the present case, the effect of rare-earth additives on the densification process was investigated. Fig. 4 shows the typical shrinkage curves (a) and the shrinkage rate curves (b) of four compositions. As shown in Fig. 4(a), the shrinkage curve is dependent on the type of additive. This tendency is clearly seen in Fig. 4(b): the shrinkage rate curve shows three peaks where the corresponding peak temperatures depend on the additives. The densification process can be divided into three stages with increasing temperature. The first peak appears between 1050 and 1300°C with a small shrinkage of about 3% for Si_3N_4–$Sm_2Si_2O_7$ and Si_3N_4–$Yb_2Si_2O_7$ compositions, and even smaller shrinkage for Si_3N_4–$Nd_2Si_2O_7$ and Si_3N_4–$Y_2Si_2O_7$ compositions. The second one occurs between

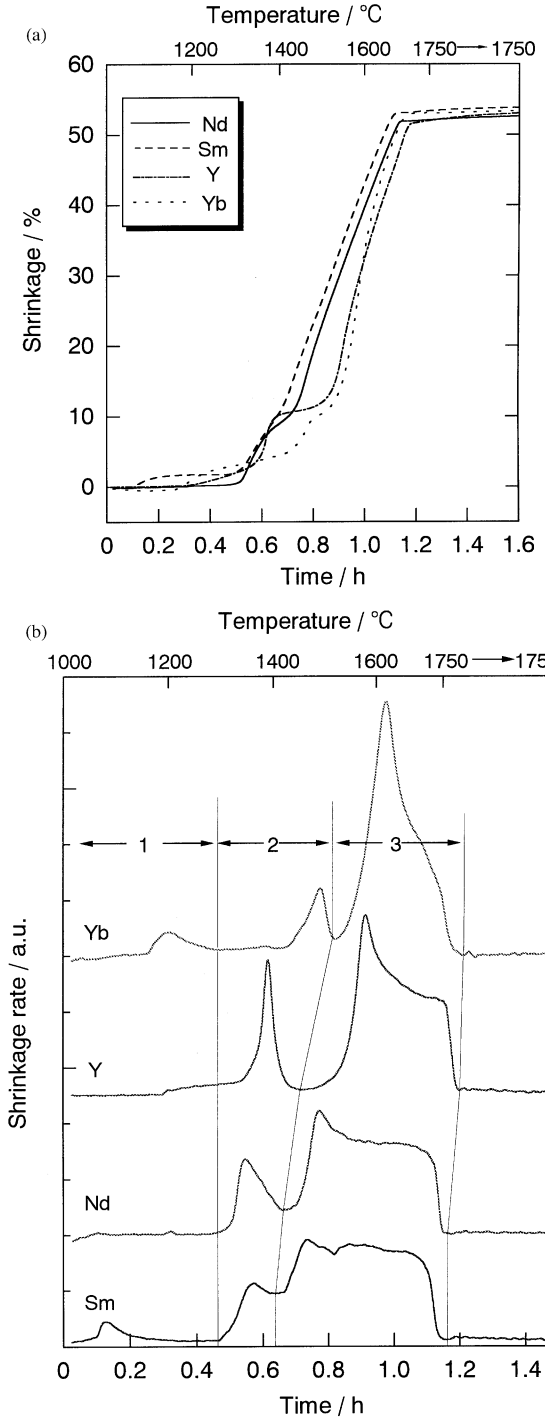

Fig. 4. (a) Shrinkage curves and (b) shrinkage rate curves of Si_3N_4–$Re_2Si_2O_7$ ceramics with different Re_2O_3 additives.

1300 and 1520°C with a shrinkage of about 7%. The last one appears from 1420 to 1750°C and has the largest shrinkage of about 42%. As shown in Fig. 4(b), the onset temperature of the final shrinkage stage is in the order of Sm < Nd < Y < Yb.

In order to clarify the reactions that occurred in these shrinkage stages, XRD measurement was carried out for samples quenched from the corresponding temperatures.

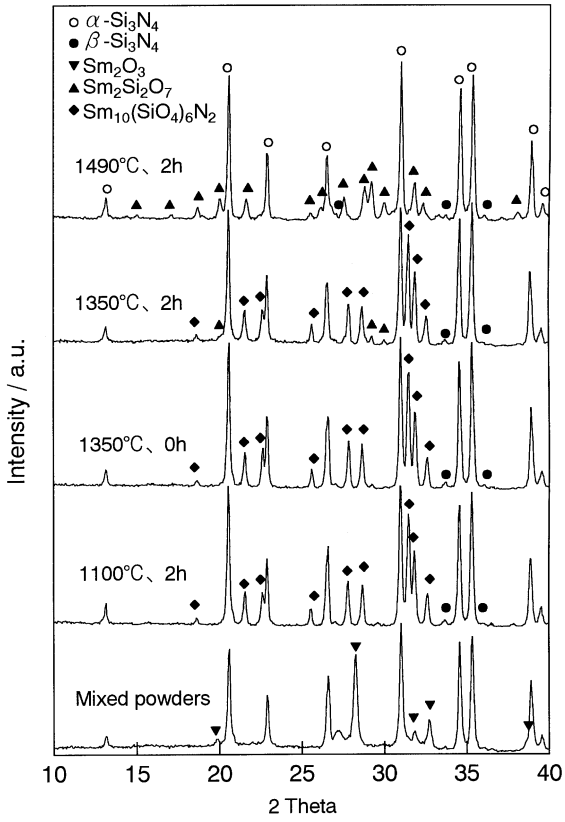

Fig. 5. XRD patterns of mixed powders and quenching samples quenched from 1100, 1350, 1490°C for Si_3N_4–$Sm_2Si_2O_7$ composition.

Fig. 5 shows an example of XRD patterns in Si_3N_4–Sm_2O_3–SiO_2 compacts quenched from various temperatures of 1100–1490°C. The data from the mixed starting powder are also shown for comparison. As shown in Fig. 5, after heating at 1100°C for 2 h, Sm_2O_3 disappeared and $Sm_{10}(SiO_4)_6N_2$ (apatite phase) appeared. At 1350°C, no $Sm_2Si_2O_7$ phase was detected. The $Sm_2Si_2O_7$ phase appeared after 2 h holding at 1350°C without a change of peak intensity of $Sm_{10}(SiO_4)_6N_2$ phase. Furthermore, at 1490°C which is in the range of the final shrinkage stage, the $Sm_{10}(SiO_4)_6N_2$ phase decreased and finally disappeared after 2 h holding while the $Sm_2Si_2O_7$ phase became the main secondary phase. The reaction sequence based on the XRD results is similar in present materials.

The result implies that the first shrinkage stage is associated with initial compaction of the powder upon the formation of the $Sm_{10}(SiO_4)_6N_2$ phase. The formation reaction of $Sm_{10}(SiO_4)_6N_2$ can be described as:

$$5Sm_2O_3 + 1/2Si_3N_4 + 9/2SiO_2 = Sm_{10}(SiO_4)_6N_2 \quad (1)$$

Although no result has been reported about the formation temperature of the initial eutectic liquid phase in the Si_3N_4–$Sm_2Si_2O_7$ composition, the present XRD results show that $Sm_2Si_2O_7$ phase appeared only after 2 h holding at 1350°C. An initial liquid phase must be formed at this temperature, and then the $Sm_2Si_2O_7$ phase crystallizes

from the liquid phase. This liquid phase must be related to the second shrinkage stage at 1350°C. On the other hand, the evidence about the formation of initial liquid phase during the secondary shrinkage stage was demonstrated in the well studied Y_2O_3-fluxed composition. Hwang et al. [13] reported that a shrinkage of about 4% at 1340°C is caused by the eutectic liquid formed at 1350°C in SiO_2–Al_2O_3–Y_2O_3 system. This shrinkage is related to the rearrangement process on the presence of an initial eutectic Si–Al–Y–O liquid without nitrogen.[14] As shown in Fig. 4(b), the peak temperature of the present Si_3N_4–$Y_2Si_2O_7$ composition is about 1400°C, which is close to the eutectic phase formation temperature of 1440°C reported in Y_2O_3–SiO_2–Si_3N_4 triangle.[13] Based on the similarity of shrinkage and temperature, a similar conclusion can be derived for present Si_3N_4–$Y_2Si_2O_7$ composition. Therefore, the intermediate shrinkage of about 7% occurred in present four compositions from 1300 to 1520°C must be related to the rearrangement process on the presence of an nitrogen free initial eutectic liquid.

As shown in Fig. 4(a), the volume shrinkage in final shrinkage stage is about 40%. It is typical of densification of a liquid-containing powder compact during the liquid phase sintering.[15] XRD results shown in Fig. 5 revealed that $Sm_{10}(SiO_4)_6N_2$ phase decreased and finally disappeared after 2 h at this temperature. It demonstrates that $Sm_{10}(SiO_4)_6N_2$ phase dissolves and nitrogen contained Si–Sm–O:-N liquid phase forms at this temperature. Therefore, in the present case, the Si–Re–O:-N liquid phase formation temperature can be estimated from the onset temperature of the final shrinkage stage where the nitrogen dissolves into the initial eutectic liquid. From the shrinkage rate curves shown in Fig. 4(b), the Si–Re–O:-N liquid phase formation temperatures of Si_3N_4–$Nd_2Si_2O_7$, Si_3N_4–$Sm_2Si_2O_7$, Si_3N_4–$Y_2Si_2O_7$ and Si_3N_4–$Yb_2Si_2O_7$ compositions can be estimated as follows: 1452, 1418, 1506 and 1542°C, respectively.

According to the network theory for glass structure,[16] the trivalent rare earth ion acts as a network intermediate. The Re–O bonds, which represent the difference of Si–Re–O–N (Re: Nd, Sm, Y, Yb) glass structure, is the weakest bond in the glass structure because the cationic radius of the rare-earth additive is the largest and the ionic charge (3^+) is lower than that of silicon cation (4^+).[17] Previous study showed that the glass properties such as glass transition temperature, softening temperature, and Young's modulus depend on the weakest bond strength.[18–20] Therefore, it is reasonable to suggest that the difference of melting temperature in the present four Si–Re–O–N glasses is caused by the Re–O bond strength. The bond strength is characterized as a field strength and its effect on the glass properties can be quantified simply by introducing the relative field strength (F_R).[21] Table 2 lists calculated relative field strength (F_R) values, that is the ratio of the field strength of the Re–O bond to that of the Nd–O bond. As shown in Table 2, when all rare earth ions exist as a trivalent state, the relative field strength (F_R) is 1.00, 1.04, 1.10 and 1.12 for the Nd–O, Sm–O, Y–O and Yb–O bonds, respectively. The values of F_R are in the order of Nd < Sm < Y < Yb which implies the Re–O bond strength is in the order of Nd < Sm < Y < Yb if rare-earth ions exist as a trivalent state. This order is due to the ionic radius, because the field strength is proportional to the ionic charge and the reciprocal of the ionic radius. On the other hand, as shown in Table 2, the relative field strength of the Sm–O bond becomes 0.69 when Sm exists as a divalent state. This may be the real situation because Sm tends to exist as a divalent state under reducing atmosphere with dissolved nitrogen in the liquid phase.[22] Thus, when Sm exists partially as a divalent state, the sequence of liquid phase formation temperature will be in the order of bond strength: Sm < Nd < Y < Yb. This is the result obtained in this study.

Table 2
Ionic radii and relative field strength (F_R) of the Re–O bond in Re–O–Si–N liquid phase

Ionic species	Ionic radius[a] (nm)	Bond	Relative field strength
O^{2-}	0.140		
Nd^{3+}	0.100	Nd–O	1.00
Sm^{3+}	0.095	Sm–O	1.04
Sm^{2+}	0.096	Sm–O	0.69
Y^{3+}	0.089	Y–O	1.10
Yb^{3+}	0.086	YB–O	1.12

[a] From Shannon (coordination number: 6).[31]

The rare-earth additives affect not only the densification process but also the high temperature strength. Fig. 6 shows the temperature dependence of flexural strength in the four materials. At room temperature, the

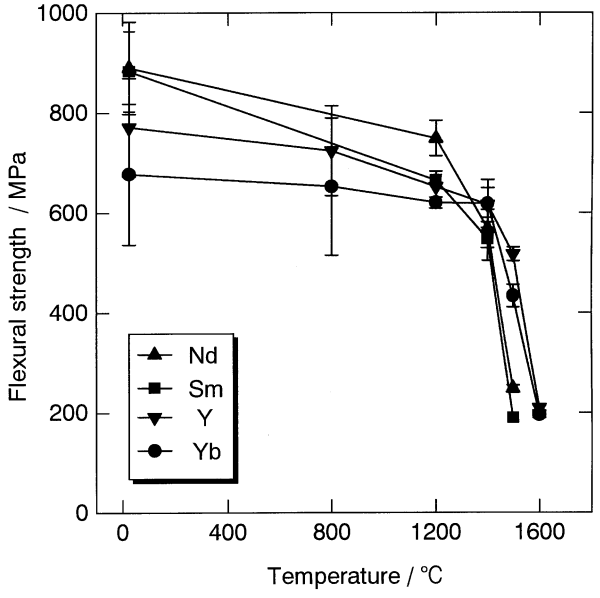

Fig. 6. Flexural strength vs testing temperature for four kinds of Si_3N_4–$Re_2Si_2O_7$ ceramics (Re: Nd, Sm, Y, Yb).

flexural strength is in the range 700–900 MPa. The value is a typical one in HP sintered silicon nitride.[23,24] The room temperature strength in Si_3N_4–$Nd_2Si_2O_7$ or Si_3N_4–$Sm_2Si_2O_7$ ceramics is higher than that of Si_3N_4–$Y_2Si_2O_7$ or Si_3N_4–$Yb_2Si_2O_7$ ceramics. This tendency is maintained up to 1200°C, but reversed above 1400°C. The flexural strength in Si_3N_4–$Y_2Si_2O_7$ ceramics at 1500°C is about 520 MPa, which is a high strength in comparison with previous reports.[5,24] The strength in Si_3N_4–$Nd_2Si_2O_7$ or Si_3N_4–$Sm_2Si_2O_7$ ceramics at 1500°C is about 220 MPa, which is 300 MPa lower than that of Si_3N_4–$Y_2Si_2O_7$ or Si_3N_4–$Yb_2Si_2O_7$ ceramics. Obviously, high temperature strength of Si_3N_4–$Y_2Si_2O_7$ or Si_3N_4–$Yb_2Si_2O_7$ ceramics is better than that of Si_3N_4–$Nd_2Si_2O_7$ or Si_3N_4–$Sm_2Si_2O_7$ ceramics.

The results of strength retention data at various testing temperature are shown in Fig. 7. The strength retention in Si_3N_4–$Nd_2Si_2O_7$ or Si_3N_4–$Sm_2Si_2O_7$ ceramics is rapidly reduced at temperatures above 1200°C. This rapid degradation of strength is due to the softening of the intergranular phase[5]. On the other hand, the strength retention in Si_3N_4–$Y_2Si_2O_7$ or Si_3N_4–$Yb_2Si_2O_7$ ceramics is rapidly reduced at temperatures above 1400°C which is about 200°C higher than that in Si_3N_4–$Nd_2Si_2O_7$ or Si_3N_4–$Sm_2Si_2O_7$ ceramics. The difference of strength retention between Si_3N_4–$Sm_2Si_2O_7$ or Si_3N_4–$Yb_2Si_2O_7$ ceramics becomes large with increasing temperature from 1200 to 1500°C. The strength retention at 1200, 1400, and 1500°C in the present materials has the order of $Sm < Nd < Y < Yb$. The above results demonstrate that the high temperature strength and strength retention depend on the types of additives.

Various models, such as cavitation mechanism,[25] solution-reprecipitation mechanism[26,27] and viscous-flow mechanism,[28,29] have been proposed to explain the high temperature deformation behavior in glass-bonded Si_3N_4 materials. These models revealed a common feature: the importance of the amorphous grain boundary phase in the high temperature deformation process. Because the high temperature strength corresponds to the phenomena of crack propagation along the grain boundary, therefore, the high temperature strength is affected by the characteristics of the amorphous intergranular film. This suggestion was supported by previous studies, that the high temperature mechanical properties must be mainly determined by the chemistry and structure of the amorphous grain boundary phase.[10,30] In the present materials, the crystallization of $Re_2Si_2O_7$ -phase with high melting temperatures occurred only at multi-grain junctions. Most two-grain boundaries remain as a glassy phase. A typical HREM image in the present materials is shown in Fig. 8. The amorphous phase with about one nanometer thickness is present in the Si_3N_4–$Y_2Si_2O_7$ interface. Though the detailed structure of the amorphous phase has not been clarified yet, the main difference of the chemistry and structure of the amorphous phase in the present four materials is the weakest Re–O bond in the structure. Therefore, it is reasonable to assume that the difference of the weakest Re–O bond strength in the amorphous phase must be an important factor for the difference of high temperature strength behavior in the present four materials. The present results support this conclusion. As shown in Fig. 7, the

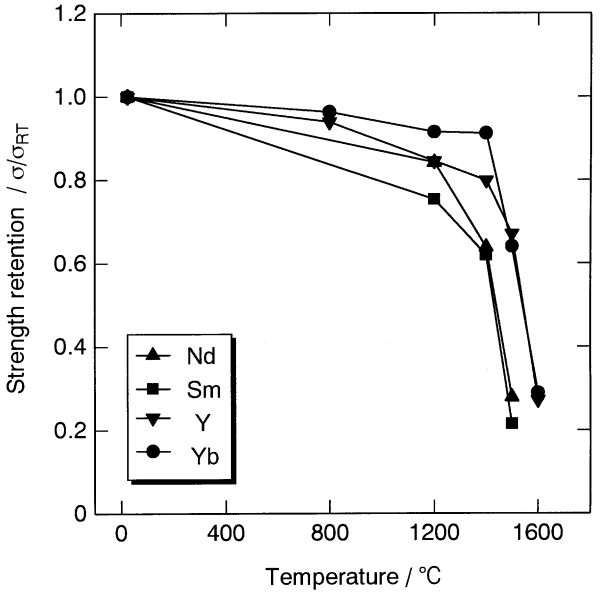

Fig. 7. Strength retention as a function of temperature for Si_3N_4–$Re_2Si_2O_7$ ceramics (Re: Nd, Sm, Y, Yb).

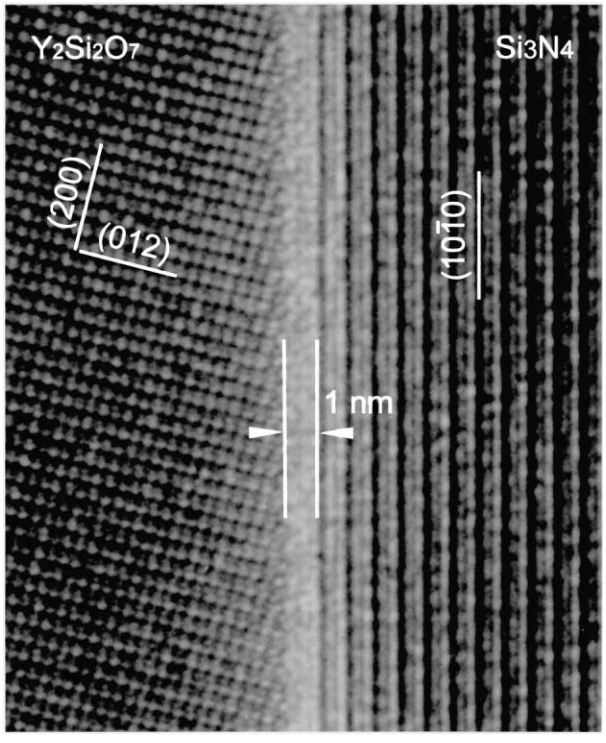

Fig. 8. HREM image showing the existence of amorphous phase in Si_3N_4–$Y_2Si_2O_7$ interface, showing a film thickness of about 1.0 nm.

strength retention at 1200°C is in the order of Sm < Nd < Y < Yb which is due to the Re–O bond strength difference (see Table 2).

As discussed above, the order of liquid phase formation temperature follows the sequence of Re–O bond strength too. Thus, the strength retention and liquid phase formation temperature may be well correlated. The relation between strength retention at 1200, 1400 and 1500°C with the liquid phase formation temperature is plotted in Fig. 9. As shown in Fig. 9, there is a roughly linear relation between the strength retention and liquid phase formation temperature. With increasing liquid phase formation temperature from 1418°C of Si_3N_4–$Sm_2Si_2O_7$ compacts to 1542°C of Si_3N_4–$Yb_2Si_2O_7$ compacts, the strength retention increased from 0.75 to 0.92 at 1200°C, 0.62 to 0.91 at 1400°C, 0.21 to 0.64 at 1500°C, respectively. On the other hand, the slope is temperature-dependent. It becomes larger with increasing testing temperature from 1200 to 1500°C.

The present results revealed that, firstly, the strength retention could be improved by adopting the additive with high liquid phase formation temperature. In other words, it is effective to improve the high temperature strength by adopting the additives with small ionic radius and high ionic charge, for example, Y_2O_3, Yb_2O_3 and Lu_2O_3. Second, the slope is temperature-dependent. This can be explained by the softening effect of the intergranular phase because the softening temperature of the intergranular film varies when the Re–O bond strength changes among the present four materials. As 1200°C is lower than the softening temperature in the present four materials, the slope has the smallest value which mainly reflects the effect of the Re–O bond strength. At 1400°C,

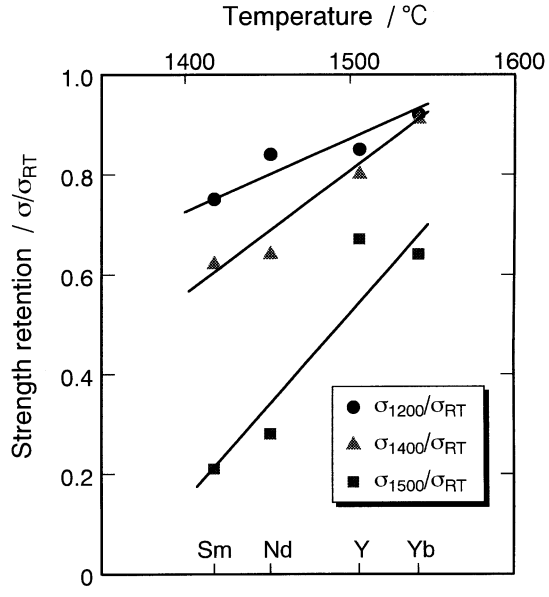

Fig. 9. The relation between the strength retention and the liquid phase formation temperature estimated from the shrinkage rate curves in Si_3N_4–$Re_2Si_2O_7$ ceramics (Re: Nd, Sm, Y, Yb).

in Si_3N_4–$Sm_2Si_2O_7$ or Si_3N_4–$Nd_2Si_2O_7$ ceramics, the fast degradation of the high temperature strength implies that the amorphous intergranular phase softens and its viscosity drops. Nevertheless, the softening of the amorphous intergranular phase in the Si_3N_4–$Y_2Si_2O_7$ or Si_3N_4–$Yb_2Si_2O_7$ ceramics is not so obvious at 1400°C because their strength is rather retained. Therefore, the slope at 1400°C is larger than that at 1200°C because of the effect of the viscosity change. At 1500°C, although the amorphous phase in Si_3N_4–$Y_2Si_2O_7$ or Si_3N_4–$Yb_2Si_2O_7$ ceramics seems to soften to a large extent, their strength retentions are 0.64 and 0.62, respectively. But the amorphous phase in Si_3N_4–$Sm_2Si_2O_7$ or Si_3N_4–$Nd_2Si_2O_7$ ceramics completely softens and their strength retentions decrease to about 0.2. Thus, the slope at 1500°C is larger than that at 1400°C.

It is well known that high temperature strength can be improved with refractory additives such as Y_2O_3 and Yb_2O_3. The present result on the relation between strength retention and liquid phase formation temperature affords a new view point to improve the high temperature strength in Si_3N_4 ceramics. The high temperature strength retention can be improved by adopting the additives with small ionic radius and high ionic charge.

4. Conclusions

(1) In the present Si_3N_4–$Re_2Si_2O_7$ (Re: Nd, Sm, Y, Yb) ceramics, densification process undergoes mainly three stages with increasing temperature. The rare-earth oxides affect the densification process of Si_3N_4–$Re_2Si_2O_7$ ceramics in which the shrinkage temperature varies with the types of rare-earth additives.

(2) The Si–Re–O–N liquid phase formation temperature, which can be estimated from the onset temperature in the final shrinkage stage, is in the order of Sm < Nd < Y < Yb, in the order of the sequence of the Re–O bond strength in the liquid phase.

(3) The effect of rare-earth oxides on the strength retention is in the sequence of Sm < Nd < Y < Yb which is similar to the order of liquid phase formation temperature. Moreover, there is roughly a linear relation between the strength retention and the liquid phase formation temperature. The present results suggest that adopting additives with a small cation radius and high ionic charge is effective to fabricate silicon nitride with high strength retention.

Acknowledgements

We wish to express gratitude to the Ministry of Education, Science and Culture, Japan for the financial support by a Grant-in-Aid for Developmental Scientific Research, Grant No. (2)-1045 0254, for Fundamental

Science Research. The authors thank N. Hirosaki, H. Tanaka, G.D. Zhan and R.J. Xue for assistance with specimen preparation and flexural strength testing.

References

1. Mitomo, M., Pressure sintering of Si_3N_4. *J. Mater. Sci.,* 1976, **11**, 1103–1107.
2. Huseby, I. C. and Petzow, G., Influence of various densifying additives on Hot-pressed Si_3N_4. *Powder Met. Int.,* 1974, **6**, 17–19.
3. Hirosaki, N., Okada, A. and Matoba, K., Sintering of Si_3N_4 with the addition of rare-earth oxides. *J. Am. Ceram. Soc.,* 1988, **71**(3), c144–c147.
4. Bonnell, D. A., Tien, T. Y. and Ruhle, M., Controlled crystallization of the amorphous phase in silicon nitride ceramics. *J. Am. Ceram. Soc.,* 1987, **70**(7), 460–465.
5. Nishimura, T., Mitomo, M., Ishida, A., Yoshida, H., Ikuhara, Y. and Sakuma, T., Heat resistant silicon nitride with ytterbium silicon oxynitride. In *6th International Symposium on Ceramic Materials and Components for Engines*, 1997, pp. 632–637.
6. Mitomo, M., Kuramoto, N. and Inomata, Y., Fabrication of high strength β-Sialon by reaction sintering. *J. Mater. Sci.,* 1979, **14**, 2309–2316.
7. Lange, F. F., Davis, B. I. and Graham, H. C., Compressive creep and oxidation resistance of an Si_3N_4 material fabricated in the system Si_3N_4–Si_2ON_2–$Y_2Si_2O_7$. *J. Am. Ceram. Soc.,* 1983, **66**, c98–c99.
8. Mieskowski, D. M. and Sanders, W. A., Oxidation of silicon nitride sintered with rare-earth oxide additions. *J. Am. Ceram. Soc.,* 1985, **68**(7), c160–c163.
9. Cinibulk, M. K., Thomas, G. and Johnson, S. M., Strength and creep behavior of rare-earth disilicate nitride ceramics. *J. Am. Ceram. Soc.,* 1992, **75**(8), 2050–2055.
10. Choi, H.-J., Lee, J.-G. and Kim, Y.-W., High temperature strength and oxidation behavior of hot-pressed silicon nitride-disilicate ceramics. *J. Mater. Sci.,* 1997, **32**, 1937–1942.
11. Nishimur, T. and Mitomo, M., Phase relationships in the system Si_3N_4–SiO_2–Yb_2O_3. *J. Mater. Res.,* 1995, **10**(2), 240–242.
12. Hirosaki, N., Akimune, Y. and Mitomo, M., Quantitative analysis of microstructure of self-reinforced silicon nitride ceramics. *J. Ceram. Soc. Jpn.,* 1993, **101**(11), 1239–1243.
13. Hwang, S.-L. and Cheng, I.-W., Reaction hot pressing of α′ and β′ -SiAlON ceramics. *J. Am. Ceram. Soc.,* 1994, **77**(1), 165–171.
14. Abe, O., Sintering process of Y_2O_3-added Si_3N_4. *J. Mater. Sci.,* 1990, **25**, 3641–3648.
15. Kingery, W. D., Woulbroun, J. M. and Charvat, F. R., Effect of applied pressure on densification during sintering in the presence of a liquid phase. *J. Am. Ceram. Soc.,* 1963, **46**(8), 391–395.
16. Vogel, W., *Glass Chemistry*, 2nd edn. Springer-Verlag, Berlin, 1995 pp. 45–48.
17. Shelby, E. and Kohli, J. T., Rare-earth aluminosilicate glasses. *J. Am. Ceram. Soc.,* 1990, **73**(1), 39–42.
18. Ohashi, M., Nakamura, K., Hitao, K., Kanzaki, S. and Hampshire, S., Formation and properties of Ln–Si–O–N glasses (Ln = Lanthanides or Y). *J. Am. Ceram. Soc.,* 1995, **78**(1), 71–76.
19. Zhang, E., Liddell, K. and Thomson, D. P., Glass formation regions and thermal expansion of some Ln–Si–Al–O–N glasses (Ln = La, Nd). *Br. Ceram. Trans.,* 1996, **95**(4), 169–172.
20. Ramesh, R., Nester, F., Pomeroy, M. J. and Hampshire, S., Formation of Ln–Si–Al–O–N glasses and their properties. *J. Eur. Ceram. Soc.,* 1997, **17**(1), 1933–1939.
21. Choi, H.-J., Kim, G.-H., Lee, J.-G. and Kim, Y.-W., Refined continumum model on the behavior of intergranular films in silicon niride ceramics. *J. Am. Ceram. Soc.,* 2000, **83**(11), 2821–2827.
22. Erying, L., *Handbook on the Physics and Chemistry of Rare Earths,* Vol. 2, ed. K. A. Gschneidner and L. R. Eyring. North Holland, Amsterdam 1979, pp. 575–577.
23. Ziegler, G., Heinrich, J. and Wotting, G., Relationships between processing, microstructure and properties of dense and reaction-bonded silicon nitride. *J. Mater. Sci.,* 1987, **22**, 3041–3086.
24. Smith, J. T. and Quackenbush, C. L., Phase effects in Si_3N_4 containing Y_2O_3 or CeO_2: strength. *Am. Ceram. Soc. Bull.,* 1980, **59**(5), 529–532,537.
25. Marion, J. E., Evans, A. G. and Drory, M. D., High temperature failure initiation in liquid phase sintered materials. *Acta Metall.,* 1983, **31**(10), 1445–1457.
26. Raj, R. and Chyung, C. K., Solution-precipitation creep in glass ceramics. *Acta Metall.,* 1981, **29**, 159–166.
27. Wakai, F., Step model of solution-precipitation creep. *Acta Metall. Mater.,* 1994, **42**(4), 1163–1172.
28. Chadwick, M. M. and Wilkinson, D. S., Creep due to a non-newtonian grain boundary phase. *J. Am. Ceram. Soc.,* 1992, **75**(9), 2327–2334.
29. Wilkinson, D. S., Creep mechanisms in multiphase ceramic materials. *J. Am. Ceram. Soc.,* 1998, **81**(2), 275–299.
30. Kleebe, H. J., Pezzotti, G. and Ziegler, G., Microstructure and fracture toughness of ceramics: combined roles of grain morphology and secondary phase chemistry. *J. Am. Ceram. Soc.,* 1999, **82**(7), 1857–1867.
31. Shannon, R. D., Revised effective ionic radii and systematic studies of interatomic distances in halides and chalcogenides. *Acta Crystallogr., Sect. A: Cryst. Phys., Diffr., Theor., Gen. Crystallogr.,* 1976, **A32**, 751–767.